

# Mass Function of Rich Galaxy Clusters and Its Constraint on $\sigma_8$

Z. L. Wen<sup>1\*</sup>, J. L. Han<sup>1</sup> and F. S. Liu<sup>2</sup>

<sup>1</sup>National Astronomical Observatories, Chinese Academy of Sciences, 20A Datun Road, Chaoyang District, Beijing 100012, China

<sup>2</sup>College of Physics Science and Technology, Shenyang Normal University, Shenyang 110034, China

Accepted 2009 ... Received 2009 ...

## ABSTRACT

The mass function of galaxy clusters is a powerful tool to constrain cosmological parameters, e.g., the mass fluctuation on the scale of  $8 h^{-1}$  Mpc,  $\sigma_8$ , and the abundance of total matter,  $\Omega_m$ . We first determine the scaling relations between cluster mass and cluster richness, summed  $r$ -band luminosity and the global galaxy number within a cluster radius. These relations are then used to two complete volume-limited rich cluster samples which we obtained from the Sloan Digital Sky Survey (SDSS). We estimate the masses of these clusters and determine the cluster mass function. Fitting the data with a theoretical expression, we get the cosmological parameter constraints in the form of  $\sigma_8(\Omega_m/0.3)^\alpha = \beta$  and find out the parameters of  $\alpha = 0.40\text{--}0.50$  and  $\beta = 0.8\text{--}0.9$ , so that  $\sigma_8 = 0.8\text{--}0.9$  if  $\Omega_m = 0.3$ . Our  $\sigma_8$  value is slightly higher than recent estimates from the mass function of X-ray clusters and the Wilkinson Microwave Anisotropy Probe (WMAP) data, but consistent with the weak lensing statistics.

**Key words:** galaxies: clusters: general — cosmological parameters

## 1 INTRODUCTION

Precise determination of cosmological parameters is an important goal in astrophysics. In the linear theory, the present root-mean-square (rms) mass fluctuation on the scale of  $8 h^{-1}$  Mpc,  $\sigma_8$ , is one of fundamental parameters (see Spergel et al. 2003) to describe the power spectrum of mass fluctuations in the universe. It is one of key parameters in the large scale structure simulations (e.g., Jenkins et al. 1998). The  $\sigma_8$  can be determined by galaxy-galaxy correlations (e.g., Tegmark et al. 2004; Cole et al. 2005), fluctuations in the cosmic microwave background (Spergel et al. 2003, 2007; Komatsu et al. 2009), gravitational lensing statistics (e.g., Hoekstra et al. 2006; Kitching et al. 2007; Benjamin et al. 2007), cluster mass function (e.g., White et al. 1993; Bahcall & Fan 1998; Reiprich & Böhringer 2002),  $\text{Ly}\alpha$  forest (Jena et al. 2005; McDonald et al. 2005) and galaxy peculiar velocities (Feldman et al. 2003).

The cluster mass function can be determined by the estimated masses for a sample of clusters (e.g., Dahle 2006), or by the X-ray luminosity and temperature function with a prior scaling relation (Viana & Liddle 1996; Allen et al. 2003). Fitting the cluster mass function with a theoretical expression can provide constraint on  $\sigma_8$ . Generally,  $\sigma_8$  is coupled with  $\Omega_m$ , the abundance of present total matter, in the form of  $\sigma_8(\Omega_m/0.3)^\alpha = \beta$ . Previous studies have found  $\alpha$  in the range 0.3–0.6 and  $\beta$  in the range 0.6–1.2 (see Table 2 in Section 4). The determined  $\sigma_8$  in recent years (2002–2009) has a

mean value of  $0.73 \pm 0.05$  assuming  $\Omega_m = 0.3$ , which is in agreement with the WMAP data (Komatsu et al. 2009), but lower than those by weak lensing statistics (Hettterscheidt et al. 2007), galaxy-galaxy correlations (Tegmark et al. 2004; Cole et al. 2005) and  $\text{Ly}\alpha$  forest (Jena et al. 2005; McDonald et al. 2005).

The amplitude of cluster mass function has large uncertainties, mainly caused by the uncertain normalization of the mass scaling relation (e.g., Henry 2004). Other uncertainties come from the scatter of mass scaling relation and the incompleteness of the X-ray flux-limited cluster samples (Reiprich & Böhringer 2002). The cluster mass function may be underestimated if only X-ray clusters are used. Erben et al. (2000) and Dahle et al. (2003) have noticed the existence of a class of X-ray-underluminous massive clusters. Popesso et al. (2007a) found that 40% of Abell clusters have a low level or no detection in X-rays. A large complete volume-limited sample of clusters is crucial for the purpose. Using the photometric redshifts of galaxies, we found 39,668 clusters in the redshift range  $0.05 < z < 0.6$  (Wen et al. 2009). Clusters are approximate volume-limited complete in the redshift range  $0.05 < z < 0.42$ . The richnesses and the summed luminosities of clusters are estimated from their luminous members, and they are tightly related to cluster mass. In Section 2, we carefully determine the scaling relation for cluster mass. In Section 3, we get the cluster mass function for a local sample of clusters and a sample at mediate redshifts, and then fit the cluster mass function with a theoretical expression for constraints on cosmological parameters,  $\Omega_m$  and  $\sigma_8$ . Discussions and conclusions are given in Section 4.

\* E-mail: zhonglue@nao.cas.cn

**Table 1.** Cluster masses from literature and the mass tracer values for 53 clusters (richness  $R \geq 8$  and  $0.03 \leq z \leq 0.3$ , sorted with  $z$ ) in the field of the SDSS DR6.

Name	R.A. (deg)	Decl. (deg)	$z$	$R$	$L_r$ ( $10^{10} h^{-2} L_\odot$ )	$GGN/r_{\text{GGN}}$ ( $\text{Mpc}^{-1}$ )	$M_{\text{vir}}$ ( $10^{14} h^{-1} M_\odot$ )	Method	Ref.
Abell 2199	247.15930	39.55121	0.030	17.76	28.49	18.10	$2.39^{+0.38}_{-0.38}$	X-ray	1
							$3.42^{+0.26}_{-0.26}$	X-ray	2
Abell 2052	229.18536	7.02162	0.035	9.50	21.97	11.62	$1.47^{+0.28}_{-0.28}$	X-ray	1
							$1.58^{+0.05}_{-0.06}$	X-ray	2
Abell 2063	230.77209	8.60922	0.035	15.30	22.96	19.93	$2.31^{+0.18}_{-0.16}$	X-ray	2
							$2.78^{+0.42}_{-0.42}$	X-ray	1
Abell 2147	240.57094	15.97465	0.035	12.22	22.50	14.67	$2.46^{+0.83}_{-0.52}$	X-ray	2
Abell 2151w	241.14914	17.72156	0.037	11.08	22.16	13.29	$1.23^{+0.09}_{-0.09}$	X-ray	2
MKW9	233.13339	4.68100	0.040	8.88	15.77	11.44	$1.01^{+0.25}_{-0.53}$	X-ray	3
Abell 1983	223.23048	16.70286	0.044	9.27	11.76	11.45	$1.06^{+0.27}_{-0.27}$	X-ray	4
							$1.39^{+0.53}_{-0.53}$	X-ray	3
Abell 160	18.24822	15.49129	0.045	16.61	34.96	16.54	$1.41^{+0.55}_{-0.55}$	X-ray	4
							$0.96^{+0.13}_{-0.14}$	X-ray	5
Abell 85	10.46029	-9.30312	0.056	23.61	54.65	21.85	$4.23^{+1.15}_{-1.15}$	X-ray	1
Abell 1991	223.63122	18.64232	0.059	19.22	39.13	17.48	$5.55^{+0.58}_{-0.53}$	X-ray	2
							$1.35^{+0.19}_{-0.53}$	X-ray	3
Abell 1795	207.21877	26.59293	0.063	19.56	39.70	19.56	$1.44^{+0.17}_{-0.17}$	X-ray	4
							$1.52^{+0.21}_{-0.21}$	X-ray	6
							$1.66^{+0.32}_{-0.24}$	X-ray	5
							$5.42^{+0.65}_{-0.65}$	X-ray	1
							$7.58^{+1.92}_{-1.70}$	X-ray	7
Abell 2092	233.31403	31.14515	0.067	9.27	15.93	11.45	$7.86^{+0.70}_{-0.70}$	X-ray	6
							$7.94^{+1.64}_{-1.51}$	X-ray	2
							$1.09^{+0.23}_{-0.20}$	X-ray	5
							$12.11^{+15.48}_{-4.88}$	X-ray	2
							$7.54^{+2.55}_{-1.91}$	X-ray	2
ZwCl 1215	184.42134	3.65584	0.075	20.69	43.81	18.71	$4.14^{+4.31}_{-1.65}$	X-ray	2
Abell 1800	207.34822	28.10732	0.075	19.77	44.73	18.83	$3.07^{+0.43}_{-0.29}$	X-ray	2
Abell 1775	205.45477	26.37347	0.076	14.52	32.62	17.76	$7.06^{+0.69}_{-0.54}$	X-ray	7
Abell 2029	227.73376	5.74478	0.077	24.87	60.63	27.47	$9.30^{+1.93}_{-1.93}$	X-ray	1
Abell 2255	258.11996	64.06072	0.080	40.23	83.40	33.51	$9.76^{+1.77}_{-1.65}$	X-ray	2
							$10.55^{+1.01}_{-1.01}$	X-ray	6
							$9.70^{+1.05}_{-0.87}$	X-ray	2
							$8.13^{+4.21}_{-2.53}$	X-ray	2
							$1.19^{+0.38}_{-0.24}$	X-ray	5
Abell 1650	194.67288	-1.76146	0.084	17.08	42.92	20.68	$4.78^{+2.64}_{-2.64}$	WL	8
Abell 1692	198.05661	-0.97448	0.085	14.40	26.42	14.73	$11.00^{+2.85}_{-1.93}$	X-ray	2
Abell 1750	202.71080	-1.86197	0.088	24.35	58.05	27.58	$11.95^{+5.24}_{-5.24}$	WL	8
Abell 2142	239.58334	27.23341	0.090	39.33	80.90	39.88	$7.23^{+9.45}_{-3.25}$	X-ray	2
Abell 2244	255.67705	34.05999	0.097	31.22	62.35	28.67	$7.17^{+4.30}_{-4.30}$	WL	8
Abell 2034	227.54883	33.48646	0.113	32.00	68.97	31.08	$4.87^{+0.42}_{-0.53}$	X-ray	3
Abell 1068	160.18541	39.95313	0.138	16.38	38.87	16.38	$5.12^{+0.45}_{-0.45}$	X-ray	4
Abell 1413	178.82501	23.40491	0.143	37.17	93.39	41.82	$5.70^{+0.57}_{-0.53}$	X-ray	3
							$5.87^{+0.59}_{-0.59}$	X-ray	4
							$8.72^{+0.80}_{-0.70}$	X-ray	2
							$9.76^{+2.54}_{-1.89}$	X-ray	7
							$9.95^{+1.04}_{-1.04}$	X-ray	6
RXJ1720.1+2637	260.04184	26.62557	0.164	26.87	69.11	27.30	$5.88^{+4.98}_{-4.60}$	WL	9
Abell 1914	216.48611	37.81645	0.171	34.16	84.15	38.07	$5.84^{+4.30}_{-4.30}$	WL	10
							$4.66^{+3.78}_{-3.49}$	WL	9
MS 0906.5+1110	137.30312	10.97475	0.176	36.00	119.08	38.61	$6.14^{+3.19}_{-3.19}$	WL	8
							$9.08^{+5.66}_{-5.66}$	WL	10
							$18.40^{+2.20}_{-1.86}$	X-ray	2
							$8.30^{+2.30}_{-2.30}$	WL	11

Table 1. – continued

Name	R.A. (deg)	Decl. (deg)	$z$	$R$	$L_r$ ( $10^{10} h^{-2} L_\odot$ )	$GGN/r_{GGN}$ ( $\text{Mpc}^{-1}$ )	$M_{\text{vir}}$ ( $10^{14} h^{-1} M_\odot$ )	Method	Ref.
Abell 1689	197.87291	−1.34108	0.184	62.74	136.85	50.32	$10.50^{+1.91}_{-1.91}$	WL	12
							$11.69^{+1.80}_{-1.80}$	SL+WL	13
							$13.24^{+3.99}_{-3.99}$	X-ray	14
							$13.43^{+0.93}_{-0.96}$	X-ray	2
							$13.51^{+1.40}_{-1.40}$	WL	15
							$14.70^{+1.40}_{-1.40}$	WL	16
							$17.55^{+3.04}_{-3.04}$	WL	17
							$20.53^{+1.74}_{-1.74}$	WL	18
							$25.50^{+5.30}_{-4.50}$	WL	11
							Abell 963	154.26515	39.04705
$6.50^{+2.00}_{-1.90}$	WL	11							
$6.53^{+2.00}_{-2.00}$	X-ray	14							
$7.00^{+2.45}_{-1.60}$	X-ray	7							
$8.01^{+8.14}_{-6.36}$	WL	9							
$8.38^{+7.46}_{-7.46}$	WL	10							
$14.98^{+7.67}_{-7.67}$	WL	10							
Abell 1423	179.32219	33.61092	0.214	20.78	64.82	21.16	$15.10^{+9.40}_{-4.30}$	X-ray	7
							$10.63^{+3.27}_{-3.27}$	X-ray	14
RX J1504.1−0248	226.03130	−2.80460	0.215	20.08	73.32	26.82			
Abell 773	139.47261	51.72704	0.217	66.83	138.50	55.08			
Abell 1682	196.70833	46.55927	0.226	40.76	112.14	39.49	$15.33^{+6.95}_{-6.95}$	WL	10
							$24.70^{+9.44}_{-11.91}$	WL	9
							$3.96^{+3.52}_{-2.40}$	WL	9
Abell 1763	203.83372	41.00115	0.228	34.10	109.20	32.77	$5.49^{+3.72}_{-3.72}$	WL	10
							$6.23^{+1.92}_{-1.92}$	X-ray	14
Abell 2219	250.08253	46.71148	0.228	45.62	94.82	45.62	$8.91^{+4.60}_{-5.70}$	WL	9
							$10.54^{+5.16}_{-5.16}$	WL	10
							$12.28^{+2.37}_{-2.37}$	WL	17
							$13.50^{+3.70}_{-3.30}$	WL	11
							$8.19^{+5.69}_{-5.69}$	WL	10
Abell 2111	234.91872	34.42426	0.229	47.58	112.27	43.38	$8.57^{+4.46}_{-5.45}$	WL	9
							$11.30^{+3.20}_{-2.70}$	WL	11
							$18.66^{+3.94}_{-3.94}$	WL	17
							$6.12^{+3.64}_{-3.64}$	WL	10
Abell 267	28.17483	1.00711	0.230	31.53	86.85	32.62	$6.92^{+3.95}_{-3.39}$	WL	9
							$2.36^{+1.29}_{-1.29}$	WL	17
							$5.36^{+1.70}_{-1.70}$	X-ray	14
Zw 1231.4+1007	188.57277	9.76623	0.231	32.00	98.28	36.99	$7.50^{+2.30}_{-2.20}$	WL	11
							$14.98^{+5.63}_{-5.63}$	WL	10
							$16.34^{+6.75}_{-6.75}$	WL	9
							$3.15^{+2.65}_{-2.65}$	WL	10
							$1.50^{+0.90}_{-0.90}$	WL	11
							$5.96^{+8.54}_{-2.70}$	X-ray	7
							$7.51^{+5.24}_{-5.24}$	WL	10
Abell 1835	210.25863	2.87846	0.252	51.57	129.59	47.96	$15.49^{+8.97}_{-9.24}$	WL	9
							$8.19^{+3.07}_{-3.07}$	WL	12
							$8.41^{+2.57}_{-2.57}$	X-ray	14
							$10.61^{+5.69}_{-5.69}$	WL	10
							$15.62^{+8.56}_{-6.35}$	WL	9
MS 1455.0+2232	224.31295	22.34288	0.258	26.00	72.03	26.00	$17.00^{+3.10}_{-3.40}$	X-ray	7
							$24.21^{+3.76}_{-3.76}$	WL	17
							$5.75^{+4.11}_{-3.26}$	WL	9
							$7.30^{+1.90}_{-1.80}$	WL	11
Abell 2631	354.41554	0.27138	0.277	46.22	113.32	44.94	$12.88^{+6.07}_{-6.07}$	WL	10
							$6.12^{+4.25}_{-4.25}$	WL	10
Abell 1758N	203.16007	50.55992	0.279	42.24	107.00	41.36	$5.26^{+5.70}_{-5.70}$	WL	8
							$26.91^{+9.57}_{-9.57}$	WL	10
							$39.09^{+12.77}_{-13.16}$	WL	9

**Table 1.** – *continued*

Name	R.A. (deg)	Decl. (deg)	$z$	$R$	$L_r$ ( $10^{10} h^{-2} L_\odot$ )	$GGN/r_{GGN}$ ( $\text{Mpc}^{-1}$ )	$M_{\text{vir}}$ ( $10^{14} h^{-1} M_\odot$ )	Method	Ref.
Abell 697	130.73982	36.36646	0.282	27.72	77.66	37.83	$22.92^{+9.78}_{-9.46}$	WL	9
							$26.10^{+9.54}_{-9.54}$	WL	10
Abell 959	154.39984	59.56710	0.285	52.77	139.82	48.82	$17.38^{+6.81}_{-6.81}$	WL	9
Abell 611	120.23674	36.05655	0.288	27.86	91.23	30.92	$6.18^{+3.82}_{-1.81}$	X-ray	7
							$6.54^{+4.43}_{-4.43}$	WL	10
							$6.90^{+5.65}_{-5.11}$	WL	9
Abell 781	140.20117	30.47176	0.288	27.17	77.19	33.22	$12.67^{+5.86}_{-5.86}$	WL	10
Zw3146	155.91515	4.18629	0.291	31.76	70.81	30.33	$11.31^{+5.44}_{-5.44}$	WL	10
							$13.99^{+7.99}_{-6.17}$	WL	9
Zw1459.4+4240	225.34604	42.34448	0.292	27.67	81.26	29.89	$10.59^{+6.00}_{-6.00}$	WL	10
Abell 1576	189.24684	63.18658	0.300	42.00	156.45	38.40	$16.01^{+6.60}_{-4.86}$	WL	9
							$18.45^{+6.03}_{-6.03}$	WL	10

Note for Method: X-ray stands for the mass determined by X-ray measurements; WL stands for weak lensing, WL+SL stands for weak lensing combined with strong lensing; References for mass estimates: [1] Xu et al. (2001), [2] Reiprich & Böhringer (2002), [3] Pointecouteau et al. (2005), [4] Arnaud et al. (2005), [5] Sun et al. (2009), [6] Vikhlinin et al. (2006), [7] Schmidt & Allen (2007), [8] Okabe & Umetsu (2008), [9] Pedersen & Dahle (2007), [10] Dahle (2006), [11] Hoekstra (2007), [12] Corless et al. (2009), [13] Limousin et al. (2007), [14] Zhang et al. (2007), [15] Broadhurst et al. (2005), [16] Umetsu & Broadhurst (2008), [17] Bardeau et al. (2007), [18] Halkola et al. (2006).

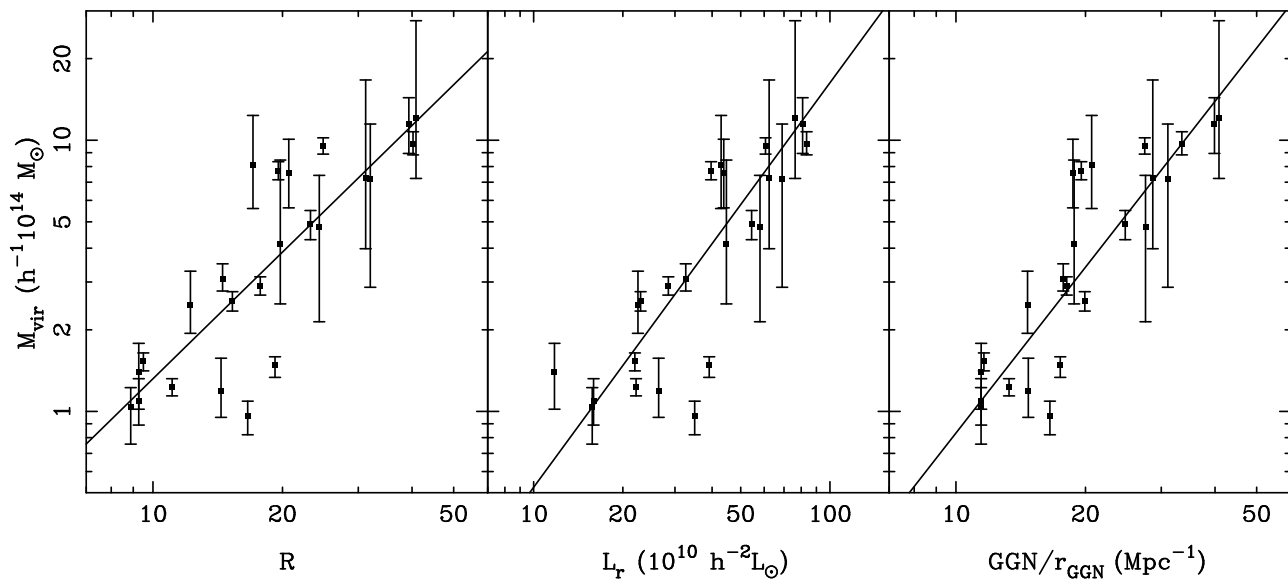


**Figure 1.** Correlations between cluster mass  $M_{\text{vir}}$  and richness  $R$ , summed luminosity  $L_r$  and  $GGN/r_{GGN}$  for 24 nearby clusters ( $R \geq 8$  and  $z \lesssim 0.1$ ). The solid line is the best fit as given in Equation (1)–(3).

Throughout this paper, we assume a flat  $\Lambda$ CDM cosmology, taking  $H_0 = 100 h \text{ km s}^{-1} \text{ Mpc}^{-1}$ , with  $h = 0.72$ ,  $\Omega_m = 1 - \Omega_\Lambda$ .

## 2 MASS SCALING RELATIONS FOR CLUSTERS

We identified 39,668 clusters from the SDSS DR6 by discrimination of luminous member galaxies with following steps (Wen et al. 2009). First, we assume that each galaxy at a given photometric redshift  $z$  is the central galaxy of a cluster candidate, and we count the number of luminous “member galaxies” of  $M_r \leq -21$  within a radius of 0.5 Mpc and a photometric redshift gap of  $z \pm 0.04(1+z)$ . We set  $\Delta z = 0.04(1+z)$  for the gap to allow variable uncertainties of photometric redshifts at different redshifts. Second, we

define the center of a cluster candidate to be the position of the galaxy with a maximum number count. The cluster redshift is estimated to be the median value of the photometric redshifts of the recognized “members”. Third, for each cluster candidate at  $z$ , all galaxies within 1 Mpc from the cluster center and  $z \pm 0.04(1+z)$  are assumed to be the member galaxies. Their absolute magnitudes are re-calculated with the cluster redshift. Finally, a cluster at  $z$  is identified when the number of member galaxies of  $M_r \leq -21$  reaches 8 within a projected radius of 0.5 Mpc and  $z \pm \Delta z$ . Monte-Carlo simulations show that the detection rate is more than 90% for massive clusters (richness  $R \geq 16.7$ ) if the redshift uncertainty of cluster galaxies is about  $0.03(1+z)$ .

We defined the cluster richness,  $R$ , to be the total number of galaxies ( $M_r \leq -21$ ) within a radius of 1 Mpc and  $z \pm 0.04(1+z)$

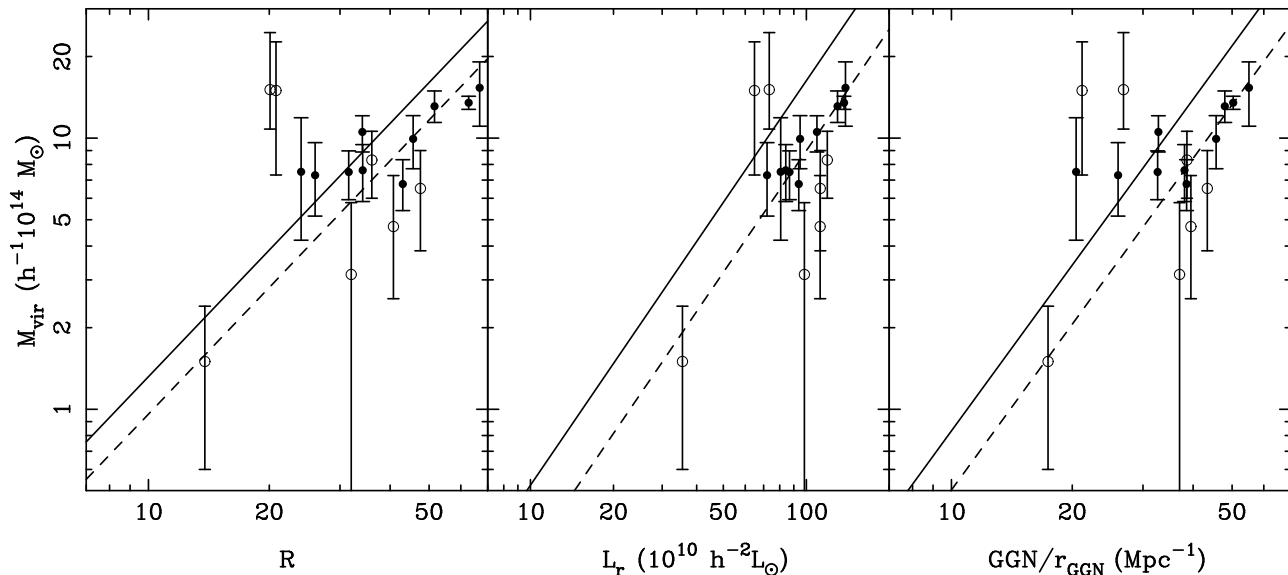


**Figure 2.** Correlations between cluster mass  $M_{\text{vir}}$  and richness  $R$ , summed luminosity  $L_r$  and  $GGN/r_{GGN}$  for 17 clusters in the redshift range  $0.17 < z < 0.26$ . The black dots are the clusters with more than three estimates of their masses. The solid lines are the same shown in Figure 1. The dashed line is the new scaling relation with the same slope but different offsets determined from the data.

after subtracting the local background, i.e., the average number of luminous galaxies. The summed  $r$ -band luminosity of each cluster,  $L_r$ , is calculated as the total luminosity of member galaxies within the region also after subtracting the background. From the radial distribution of member galaxies, we got the cluster radius,  $r_{GGN}$ , where the density of galaxies is as low as background. Here, we defined the Gross Galaxy Number ( $GGN$ ) of a cluster as the total number of luminous galaxies ( $M_r \leq -21$ ) within the radius  $r_{GGN}$  and the redshift gap of  $z \pm 0.04(1+z)$  after subtracting the local background. It has been known for a long time that the cluster richness and summed luminosity are related to cluster mass (Girardi et al. 2002; Popesso et al. 2007b), hence they can be the tracers of cluster mass. The  $GGN/r_{GGN}$  is related to the amplitude of cluster-galaxy cross-correlation since the correlation is described by  $\xi(r) \propto r^{-2}$  (e.g., Lilje & Efstathiou 1988). We find that  $GGN/r_{GGN}$  can also be the tracer of cluster richness.

Cluster mass can be determined by the velocity dispersion of member galaxies (Zwicky 1933). However, velocity measurements can be corrupted by projection effects that might be difficult to diminish in practice. The error on the individual measurements can introduce a significant bias (von der Linden et al. 2007). Under the assumption of hydrostatic equilibrium, the X-ray method can determine mass distribution of a cluster to a large radius. The assumption is invalid for clusters with substructures, inducing an underestimation of mass (Schindler 1996). Weak gravitational lensing recently becomes a sophisticated method to estimate cluster mass without assumptions on dynamical state of a cluster. The uncertainty of mass mainly comes from the difficulty in measuring the image distortions of the faint background sources. We collect the cluster masses estimated by X-ray and weak lensing methods from literature (see Table 1). Usually, cluster masses are denoted as  $M_\Delta$  which is the mass within a radius  $r_\Delta$  interior to which the mean density is  $\Delta$  times the critical density of the universe. For cosmology with  $\Omega_m = 0.3$ , the virial mass is calculated within the radius  $r_\Delta$ , here  $\Delta = 101$ , so that  $M_{\text{vir}} = M_{101}$  (Kitayama & Suto 1996). Previous studies usually provided the mass within  $r_{200}$  or  $r_{500}$  (e.g., Reiprich & Böhringer 2002; Pedersen & Dahle 2007).

Here, we convert the mass of  $M_{200}$  and  $M_{500}$  to the virial mass  $M_{\text{vir}}$  according to Shimizu et al. (2003). We will discuss later the influence on our result from a possible bias conversion. For each cluster with mass estimated, we calculate the cluster richness, the summed  $r$ -band luminosity and  $GGN/r_{GGN}$  following the method of Wen et al. (2009). Only clusters of richness  $R \geq 8$  are listed in Table 1 since the uncertainties of  $R$  and the summed luminosities become larger for clusters with a smaller  $R$ .

We notice that clusters with estimated masses preferentially have low ( $z \lesssim 0.1$ ) and mediate ( $\sim 0.2 < z < 0.25$ ) redshifts (see Table 1). To minimize the uncertainty, we determine the scaling relations between the masses and observational tracers for clusters in the two small redshift ranges independently. This is because the discrimination of member galaxies (e.g., completeness or contamination rate) may be different for clusters at different redshifts, and the systematic bias can be ignored in such a small range. In the low redshift range ( $z \lesssim 0.1$ ), the masses of many clusters are available and distributed in a large mass range, which is good for determination of the scaling relations. We get 15 clusters of  $0.05 < z < 0.1$ . We also include 8 clusters of  $0.03 < z < 0.05$  and one cluster of  $z = 0.113$  to derive the scaling relations at the low redshift range. Several clusters have multiple estimates for mass from literature, we adopt the median value or the average of two middle ones for even measurements.

The mass–richness relation, i.e., the so called halo occupation distribution in some literature (e.g., Popesso et al. 2007b), is described by a power law,  $R \propto M^\mu$ . The correlation of cluster mass with the optical luminosity, i.e., the mass-to-light ratio  $M/L$ , is also described by a power law,  $M/L \propto L^\nu$ , i.e.,  $M \propto L^{1+\nu}$ . In Figure 1, we show the correlations between cluster mass and cluster richness, summed luminosity and  $GGN/r_{GGN}$  for 24 nearby clusters. The uncertainties of richness  $R$ , summed luminosity  $L_r$  and  $GGN/r_{GGN}$  are about 10%–20% (Wen et al. 2009). We fit the correlations with power-law relations,

$$\log M_{\text{vir}} = (-1.43 \pm 0.07) + (1.55 \pm 0.06) \log R, \quad (1)$$

$$\log M_{\text{vir}} = (-1.77 \pm 0.08) + (1.49 \pm 0.05) \log L_r, \quad (2)$$

and

$$\log M_{\text{vir}} = (-2.11 \pm 0.10) + (2.03 \pm 0.08) \log(GGN/r_{GGN}). \quad (3)$$

Here,  $M_{\text{vir}}$  has a unit of  $10^{14} h^{-1} M_{\odot}$ ,  $L_r$  has a unit of  $10^{10} h^{-2} L_{\odot}$ . The uncertainty of the estimated cluster mass,  $\sigma_{\log M}$ , is mainly determined by the uncertainties of the intercept and the slope in the logarithm for three scaling relations in Equation (1)–(3). Yee & Ellingson (2003) defined  $B_{\text{gc}}$  to be the amplitude of galaxy-cluster cross-correlation function and found  $M_{\text{vir}} \propto B_{\text{gc}}^{1.64 \pm 0.28}$ . The slope is in agreement with that of our  $M_{\text{vir}}$  to  $GGN/r_{GGN}$  relation. These scaling relations, Equation (1)–(3), will be used to estimate masses of a complete volume-limited sample of clusters in the local universe for cluster mass function.

We can also use a much larger cluster sample at mediate redshift ( $\sim 0.2 < z < 0.25$ ) for cluster mass function. Some massive clusters in this redshift range have their masses estimated (see Table 1). We obtain masses of 17 clusters in the redshift range of  $0.17 < z < 0.26$ , of which 10 clusters have more than three estimates. In Figure 2, we show the correlations between cluster mass and cluster richness, summed luminosity and  $GGN/r_{GGN}$  for the 17 clusters. Most of them are similarly massive of  $10^{15} h^{-1} M_{\odot}$  and few have smaller masses, so that it is difficult to determine a new scaling relations. Here, we calibrate the mass scaling relations by assuming the same slopes of Equation (1)–(3) and finding the offsets. We then get the scaling relations,

$$\log M_{\text{vir}} = (-1.57 \pm 0.12) + 1.55 \log R, \quad (4)$$

$$\log M_{\text{vir}} = (-2.03 \pm 0.06) + 1.49 \log L_r, \quad (5)$$

and

$$\log M_{\text{vir}} = (-2.33 \pm 0.11) + 2.03 \log(GGN/r_{GGN}). \quad (6)$$

The uncertainties in Equation (4)–(6) reflect the scatters of masses to the mean relations (dashed line). We notice that the scatter is the smallest for the  $M_{\text{vir}}-L_r$  relation for the high redshift data, because clusters with more than three estimates (black dots) are very consistent with the fitting relation (dashed line). Therefore, the cluster masses estimated by the  $M_{\text{vir}}-L_r$  relation may be more accurate than other tracers. The offsets between the relations for samples at two redshift ranges may come from the problem of the SDSS galaxy data. The sky background level is overestimated for nearby bright galaxies ( $12.5 < r < 15.5$ ), so that galaxies have systematically fainter magnitudes by 0.15–0.2 mag than their true magnitude (Adelman-McCarthy et al. 2008). This can result in systematically lower cluster richness and summed luminosity for clusters of  $0.05 < z < 0.1$  than clusters of  $0.2 < z < 0.25$ . The two scaling relations are used to samples of clusters at two redshift ranges independently. Hence, the systematic bias does not affect the final  $\sigma_8$  values from each sample.

### 3 CLUSTER MASS FUNCTIONS

Assuming a Gaussian distribution of mass fluctuation, Press & Schechter (1974) used a linear theory to derive the first theoretical expression of cluster mass function, which is in agreement with mass functions derived from observations and numerical simulations within a large mass range (e.g., White et al. 1993; Reiprich & Böhringer 2002). Recent simulations show slightly more massive clusters than the Press & Schechter mass function gives (Sheth & Tormen 1999; Jenkins et al. 2001; Warren et al. 2006). In this work, we take the form of the cluster

mass function as Equation (B4) of Jenkins et al. (2001). The mean differential comoving number density of dark matter halos is

$$\frac{dn}{dM} = 0.316 \frac{\rho_0}{M^2} \frac{d \ln \sigma^{-1}}{d \ln M} \exp(-[\ln \sigma^{-1} + 0.67]^{3.82}). \quad (7)$$

Here,  $\rho_0 = 2.78 \times 10^{11} \Omega_m h^2 M_{\odot} \text{Mpc}^{-3}$  is the comoving density of the universe.  $M$  is the halo mass within a radius with a mean overdensity of 324 times of the mean density of the universe (roughly the virial mass,  $M_{101}$ , if  $\Omega_m = 0.3$ ).  $\sigma^2(M, z)$  is the variance of the linearly evolved density field smoothed by a spherical top-hat filter that enclose mass  $M$ . Here,  $\sigma(M, z) = \sigma_8 \times f$ , where  $\sigma_8$  is the present linear rms mass fluctuation on the scale of  $8 h^{-1} \text{Mpc}$  and  $f$  is a function of  $M, z, \Omega_m$  as well as the Hubble constant  $h$ , the abundance of baryons  $\Omega_b$  and the present cosmic microwave background temperature  $T_{\text{CMB}}$ .  $d \ln \sigma^{-1} / d \ln M$  can be derived from the expression of  $\sigma(M, z)$  (see details of  $\sigma(M, z)$  in Reiprich & Böhringer 2002). The values of  $\Omega_m$  and  $\sigma_8$  are the main parameters to define the mass function. The other parameters does not strongly affect the results in our analysis, thus can be fixed. The  $\sigma_8$  strongly depends on cluster mass function at the high mass end. Since the mass function is steep at high mass end, the data scatter for mass scaling relations induces more low mass to higher mass. Thus, the uncertainty of the mass scaling relation,  $\sigma_{\log M}$ , is included in the fitting. We re-write the mass function with the uncertainty on mass estimate to be the Jenkins function convolved by a Gaussian function,

$$\frac{d\tilde{n}(M)}{d \log M} = \int \frac{dn(M')}{d \log M'} g(\log M - \log M', \sigma_{\log M}) d \log M', \quad (8)$$

where  $g(x, \sigma) = e^{-x^2/2\sigma^2} / (\sqrt{2\pi}\sigma)$ .

First, we use a complete volume-limited sample of rich clusters ( $R \geq 16.7$ , 90% complete) in the local universe ( $0.05 < z < 0.1$ ) to determine the cluster mass function. Since the photometric redshift was used to identify the cluster member galaxies, the absolute magnitudes of member galaxies could have large uncertainties when the estimated cluster redshift slightly deviates from its true redshift. To reduce the uncertainty at low redshift, we use the spectroscopic redshifts of clusters if its discriminated members are spectroscopically observed. The cluster richness, the summed  $r$ -band luminosity and  $GGN/r_{GGN}$  are re-calculated as Wen et al. (2009). In this sample, 56 clusters have richness  $R \geq 16.7$ , which are used to determine the cluster mass function in the local universe.

We apply the scaling relations of Equation (1)–(3) to these 56 rich clusters in the local universe and calculate the number of clusters as a function of mass. Figure 3 shows the cluster mass functions and the best fit with Equation (8). From the probability contours in the  $\sigma_8-\Omega_m$  plane for three mass tracers (Figure 4), we find that the  $\sigma_8$  and  $\Omega_m$  are coupled in the form of  $\sigma_8(\Omega_m/0.3)^\alpha = \beta$ . From the cluster mass distribution using the mass–richness scaling relation, we find

$$\sigma_8 \left( \frac{\Omega_m}{0.3} \right)^{0.42 \pm 0.03} = 0.82 \pm 0.04. \quad (9)$$

From the cluster mass distribution using the mass–luminosity scaling relation, we find

$$\sigma_8 \left( \frac{\Omega_m}{0.3} \right)^{0.46 \pm 0.03} = 0.90 \pm 0.04. \quad (10)$$

From the cluster mass distribution using the mass– $GGN/r_{GGN}$  scaling relation, we find

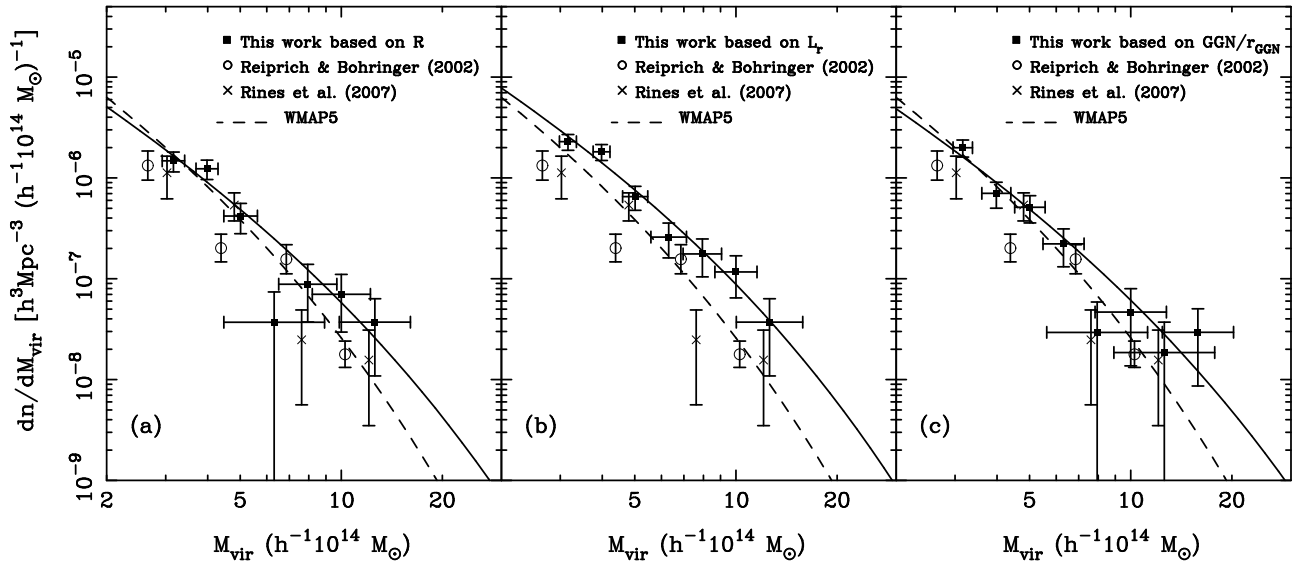


**Figure 3.** Mass function for a sample of 56 rich clusters ( $R \geq 16.7$ ,  $0.05 < z < 0.1$ ). The error bars on the horizontal axis are calculated from the uncertainties of Equation (1)–(3), and the error bars on the vertical axis are calculated by Poisson statistics. The solid line is the best fit with the cluster mass function of Equation (8). The dashed line is the cluster mass function of Equation (8) with  $\Omega_m = 0.273$  and  $\sigma_8 = 0.813$  from the WMAP5 data (Komatsu et al. 2009). Data for the mass functions from Reiprich & Böhringer (2002) and Rines et al. (2007) are plotted for comparison.

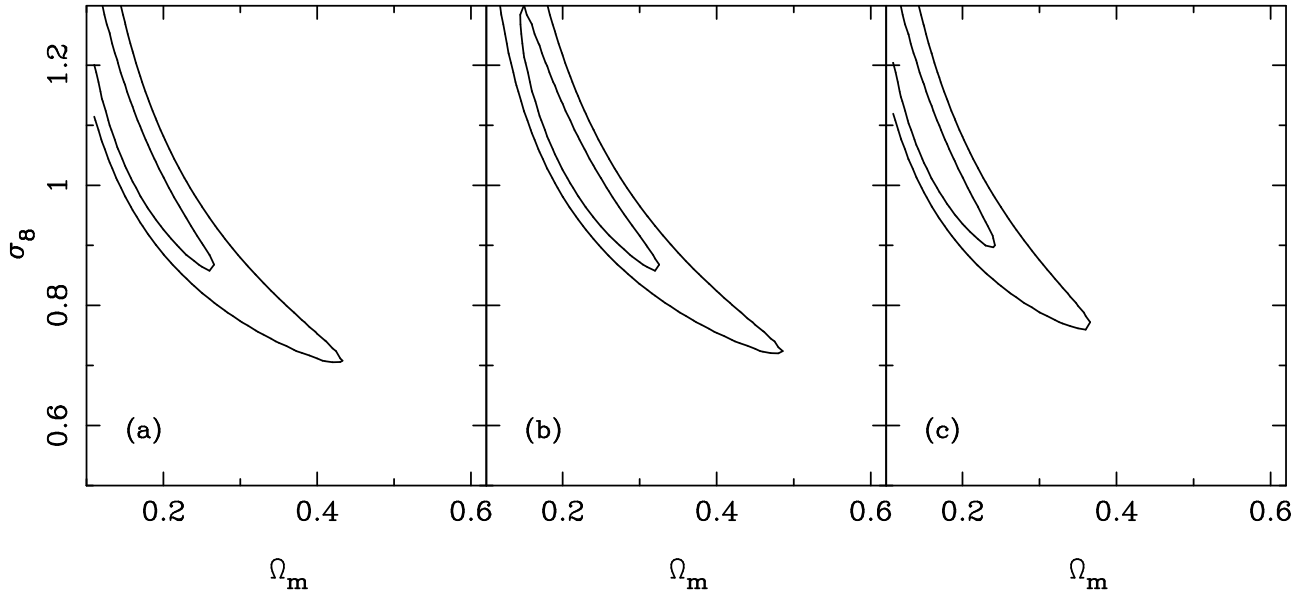


**Figure 4.** The probability contour in the  $\sigma_8$ – $\Omega_m$  plane for three corresponding mass tracers in Figure 3, 68% confidence level for the inner curve and 99% for the outer curve.

$$\sigma_8 \left( \frac{\Omega_m}{0.3} \right)^{0.40 \pm 0.03} = 0.83 \pm 0.04. \quad (11)$$

During the fitting, we have taken into account only statistical uncertainties. Assuming  $\Omega_m = 0.3$ , the value of  $\sigma_8$  is  $0.82 \pm 0.04$ ,  $0.90 \pm 0.04$  and  $0.83 \pm 0.04$  for masses scaled from cluster richness, summed luminosity and  $GGN/r_{GGN}$ , respectively.

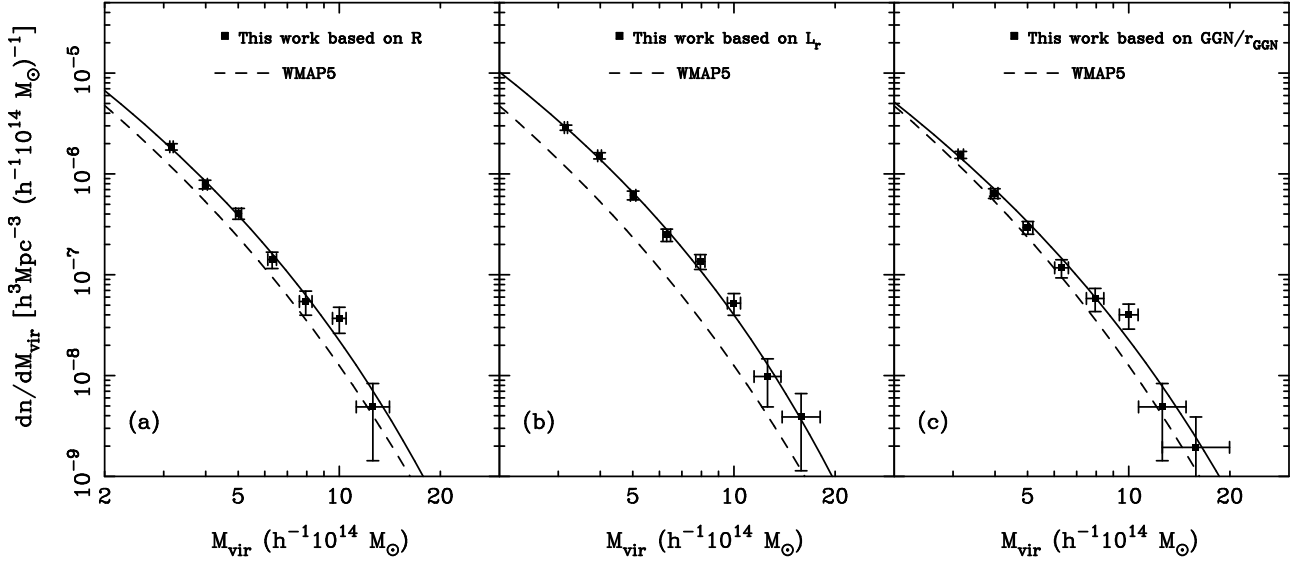
We also apply the scaling relations of Equation (4)–(6) to the a complete volume-limited sample of 810 rich clusters ( $R \geq 16.7$ ) of  $0.2 < z < 0.25$  to calculate their masses, and get the cluster mass function. Again, spectroscopic redshifts of 466 clusters are used since they are available from the SDSS, otherwise photometric redshifts are used. Figure 5 shows the cluster mass functions and

Figure 6 shows the contours in the  $\sigma_8$ – $\Omega_m$  plane based on three mass tracers. Since there are much more clusters in this sample, the mass functions have small errors than those of  $0.05 < z < 0.1$ . We fit the data to Equation (8), and find

$$\sigma_8 \left( \frac{\Omega_m}{0.3} \right)^{0.42 \pm 0.01} = 0.85 \pm 0.02, \quad (12)$$

$$\sigma_8 \left( \frac{\Omega_m}{0.3} \right)^{0.46 \pm 0.01} = 0.94 \pm 0.02, \quad (13)$$

$$\sigma_8 \left( \frac{\Omega_m}{0.3} \right)^{0.39 \pm 0.01} = 0.82 \pm 0.02, \quad (14)$$



**Figure 5.** The same as Figure 3 but for a sample of 810 rich clusters ( $R \geq 16.7$ ,  $0.2 < z < 0.25$ ). The curve from the WMAP5 result by Komatsu et al. (2009) is plotted for comparison.

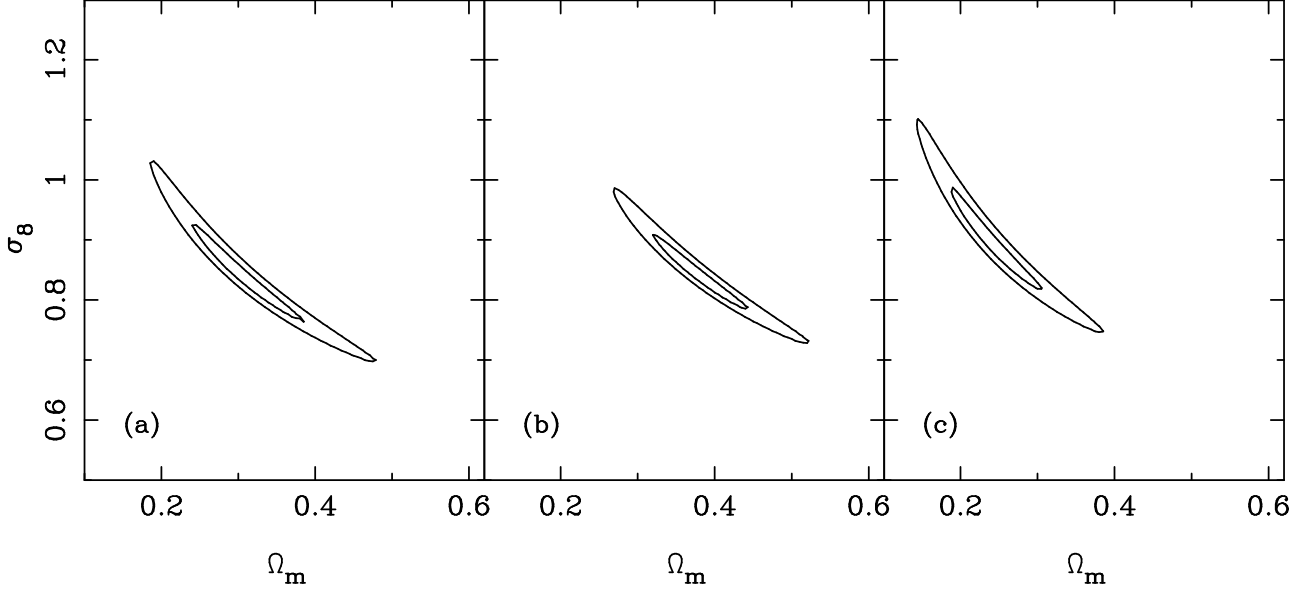


**Figure 6.** The same as Figure 4 but corresponding to the three mass tracers in Figure 5 for the cluster sample of  $0.2 < z < 0.25$ .

for the cases using the mass tracer of richness, summed luminosity and the  $GGN/r_{GGN}$ , respectively. Assuming  $\Omega_m = 0.3$ , the value of  $\sigma_8$  is  $0.85 \pm 0.02$ ,  $0.94 \pm 0.02$  and  $0.82 \pm 0.02$ , respectively. They are consistent with those from the cluster sample of  $0.05 < z < 0.1$  for each mass tracer.

#### 4 DISCUSSIONS AND CONCLUSIONS

Cluster mass function can be accurately determined from a complete volume-limited sample. The scaling relations of cluster mass have been determined for three optical observations, cluster richness, summed luminosity and  $GGN/r_{GGN}$ . The scaling relations are then used to estimate cluster mass for two samples of rich clusters. We get cluster mass functions and fit them with a theoretical

expression. Cosmological parameters are constrained in the form of  $\sigma_8(\Omega_m/0.3)^\alpha = \beta$ , with  $\alpha = 0.40\text{--}0.50$  and  $\beta = 0.8\text{--}0.9$ . For  $\Omega_m = 0.3$ , we get  $\sigma_8 = 0.8\text{--}0.9$  using different mass tracers or using the rich cluster samples at different redshift ranges.

The  $\sigma_8$  values from the mass tracers of richness  $R$  and  $GGN/r_{GGN}$  obtained using both cluster samples are consistent, while  $\sigma_8$  values derived from  $L_r$  are higher. This discrepancy may come from some potential systematic bias on the mass scaling relations. If the  $M_{vir}\text{--}L_r$  relations for both samples are really unbiased, then the cluster masses tracer by richness  $R$  and  $GGN/r_{GGN}$  are systematically underestimated. However, it is hard to assess which one is a better mass tracer. Given the scarce of mass estimates from different methods for the same clusters in Table 1 for the scaling relations, it is also hard to estimate the systematic bias on these mass estimates due to different methods (X-ray or weak lensing).



**Table 2.** Comparison of results on  $\sigma_8$ - $\Omega_m$  derived from cluster mass function (upper part) and cosmic microwave background (CMB) measurement (middle part). See Table 5 of Hettterscheidt et al. (2007) for the results derived from weak lensing statistics.

Reference	Sample or method	No. of clusters or observation	$\sigma_8$ - $\Omega_m$ relation	$\sigma_8$ ( $\Omega_m = 0.30$ )
Viana & Liddle (1996)	X-ray	25	$\sigma_8 = 0.60\Omega_m^{-0.59+0.16\Omega_m-0.06\Omega_m^2}$	1.16
Eke et al. (1996)	X-ray	25	$\sigma_8=(0.52\pm 0.04)\Omega_m^{-0.52+0.13\Omega_m}$	$0.93\pm 0.07$
Markevitch (1998)	X-ray	30	$\sigma_8 = 0.78 \pm 0.04$ with $\Omega_m = 0.30$ fixed	$0.78\pm 0.04$
Pen (1998)	X-ray	25	$\sigma_8=0.53\Omega_m^{-0.53}$	1.00
Borgani et al. (1999)	X-ray	70	$\sigma_8=0.58\pm 0.06\Omega_m^{-0.47\pm 0.16\Omega_m}$	0.96
Viana & Liddle (1999)	X-ray	10	$\sigma_8=0.56\Omega_m^{-0.47}$	0.99
Blanchard et al. (2000)	X-ray	25	$\sigma_8 = 0.96$ with $\Omega_m = 0.30$ fixed	0.96
Oukbir & Arnaud (2001)	X-ray	69	$\sigma_8=0.59\Omega_m^{-0.57+1.45\Omega_m-3.48\Omega_m^2+3.77\Omega_m^3-1.49\Omega_m^4}$	0.91
Wu (2001)	X-ray	25	$\sigma_8=0.477\Omega_m^{-0.3-0.17\Omega_m^{0.34}-0.13\Omega_m}$	0.87
Borgani et al. (2001)	X-ray	103	$\sigma_8=0.66^{+0.06}_{-0.05}, \Omega_m = 0.35^{+0.13}_{-0.10}$	-
Pierpaoli et al. (2001)	X-ray	30	$\sigma_8=(0.495^{+0.034}_{-0.037})\Omega_m^{-0.60}$	$1.02^{+0.07}_{-0.08}$
Viana et al. (2002)	X-ray	452	$\sigma_8=0.38\Omega_m^{-0.48+0.27\Omega_m}$	0.61
Reiprich & Böhringer (2002)	X-ray	106	$\sigma_8=0.43\Omega_m^{-0.38}$	0.68
Seljak (2002)	X-ray	30	$\sigma_8(\Omega_m/0.3)^{0.44} = 0.77 \pm 0.07$	$0.77\pm 0.07$
Viana et al. (2003)	X-ray	40	$\sigma_8 = 0.78^{+0.30}_{-0.06}$ with $\Omega_m = 0.35$ fixed	-
Schuecker et al. (2003)	X-ray	452	$\sigma_8=0.711^{+0.039}_{-0.031}, \Omega_m = 0.341^{+0.031}_{-0.029}$	-
Pierpaoli et al. (2003)	X-ray	63	$\sigma_8=0.77^{+0.05}_{-0.04}$ with $\Omega_m = 0.30$ fixed	$0.77^{+0.05}_{-0.04}$
Allen et al. (2003)	X-ray	111	$\sigma_8=(0.508\pm 0.019)\Omega_m^{-0.253\pm 0.024}$	$0.69\pm 0.05$
Henry (2004)	X-ray	51	$\sigma_8 = 0.66 \pm 0.16$ with $\Omega_m = 0.30$ fixed	$0.66\pm 0.16$
Dahle (2006)	X-ray	35	$\sigma_8(\Omega_m/0.3)^{0.37} = 0.67^{+0.04}_{-0.05}$	$0.67^{+0.04}_{-0.05}$
Rines et al. (2007)	X-ray	66	$\sigma_8 = 0.92^{+0.24}_{-0.19}, \Omega_m = 0.24^{+0.14}_{-0.09}$	$0.84 \pm 0.03$
Henry et al. (2009)	X-ray	48	$\sigma_8(\Omega_m/0.32)^{0.30} = 0.86 \pm 0.04$ for $\Omega_m \leq 0.32$ $\sigma_8(\Omega_m/0.32)^{0.41} = 0.86 \pm 0.04$ for $\Omega_m \geq 0.32$	$0.88\pm 0.04$
Vikhlinin et al. (2009)	X-ray	49	$\sigma_8(\Omega_m/0.25)^{0.47} = 0.813 \pm 0.027$	$0.75\pm 0.02$
White et al. (1993)	Optical		$\sigma_8 = 0.57\Omega_m^{-0.56}$	1.12
Bahcall & Fan (1998)	Optical	3	$\sigma_8\Omega_m^{0.29} = 0.8 \pm 0.1$	$1.13\pm 0.14$
Girardi et al. (1998)	Optical	152	$\sigma_8=(0.60\pm 0.04)\Omega_m^{-0.46+0.09\Omega_m}$	$1.01\pm 0.07$
Bahcall et al. (2003)	Optical	300	$\sigma_8\Omega_m^{0.60} = 0.33 \pm 0.03$	$0.68\pm 0.06$
Eke et al. (2006)	Optical		$\sigma_8=0.25\Omega_m^{-0.92-4.5(\Omega_m-0.22)^2}$	0.78
Rozo et al. (2010)	Optical	13832	$\sigma_8(\Omega_m/0.25)^{0.41} = 0.83 \pm 0.03$	$0.76\pm 0.03$
Komatsu et al. (2009)	CMB	WMAP5	$\sigma_8 = 0.81 \pm 0.03, \Omega_m = 0.27 \pm 0.01$	
Liu & Li (2009)	CMB	WMAP5	$\sigma_8 = 0.92 \pm 0.04, \Omega_m = 0.32 \pm 0.03$	
Larson et al. (2010)	CMB	WMAP7	$\sigma_8 = 0.80 \pm 0.03, \Omega_m = 0.26 \pm 0.01$	
Readhead et al. (2004)	CMB	CBI	$\sigma_8 = 0.96^{+0.06}_{-0.07}$ (68% confidence level)	
Dawson et al. (2006)	CMB	BIMA	$\sigma_8 = 1.03^{+0.20}_{-0.29}$ (68% confidence level)	
Reichardt et al. (2009)	CMB	ACBAR	$\sigma_8 = 0.93^{+0.04}_{-0.05}$	
Sievers et al. (2009)	CMB	CBI	$\sigma_8 = 0.92^{+0.05}_{-0.05}$	
Sayers et al. (2009)	CMB	Bolocam	$\sigma_8 < 1.57$ (90% confidence level)	
Veneziani et al. (2009)	CMB	BOOMERANG	$\sigma_8 < 0.92$ (95% confidence level)	
This work ( $0.05 < z < 0.1$ )	$R$	56	$\sigma_8(\Omega_m/0.3)^{0.42} = 0.82 \pm 0.04$	$0.82\pm 0.04$
	$L_r$		$\sigma_8(\Omega_m/0.3)^{0.46} = 0.90 \pm 0.04$	$0.90\pm 0.04$
	$GGN/\tau_{GGN}$		$\sigma_8(\Omega_m/0.3)^{0.40} = 0.83 \pm 0.04$	$0.83\pm 0.04$
This work ( $0.2 < z < 0.25$ )	$R$	810	$\sigma_8(\Omega_m/0.3)^{0.42} = 0.85 \pm 0.02$	$0.85\pm 0.02$
	$L_r$		$\sigma_8(\Omega_m/0.3)^{0.46} = 0.94 \pm 0.02$	$0.94\pm 0.02$
	$GGN/\tau_{GGN}$		$\sigma_8(\Omega_m/0.3)^{0.39} = 0.82 \pm 0.02$	$0.82\pm 0.02$

In our work, one potential systematic bias may come from the conversion of cluster mass from measured radii to the virial radius. Here, we use  $\gamma = M_{\text{vir}}/M_{\text{vir,true}}$  to stand for the systematic bias of masses in Table 1, where  $M_{\text{vir,true}}$  stands for the true virial mass of a cluster. Assuming a  $\gamma$ , we get  $M_{\text{vir,true}}$  and then fit the mass function of clusters to obtain  $\sigma_8$ . Figure 7 shows the variation of  $\sigma_8$  (with  $\Omega_m = 0.3$  fixed) as a function  $\gamma$  based on the  $M_{\text{vir}}-L_r$  relation. We are only concerned about the cases  $\gamma \geq 1$ . For example  $\gamma = 1.3$ , i.e., masses systematically overestimated by 30%, the

values of  $\sigma_8$  are lower by about 10%. In fact, the deviation of  $\gamma$  from 1.0 is related to the uncertainty of intercept in the logarithm scaling relations in Equation (1)–(6). The other possible systematic bias on  $\sigma_8$  may come from the slope uncertainties of the scaling relations. Here, we illustrate the dependence of  $\sigma_8$  on the slope uncertainty,  $\Delta\nu$ . We only apply to the  $M_{\text{vir}}-L_r$  relation, for example. Given a  $\Delta\nu$ , i.e.,  $M_{\text{vir}} = A L_r^{1+\nu+\Delta\nu}$ , here  $\nu = 1.49$  according to Equation (2) and (5), we fit the power law with the data in Figure 1 and 2 to get  $A$ , and then get the cluster mass function and fit for

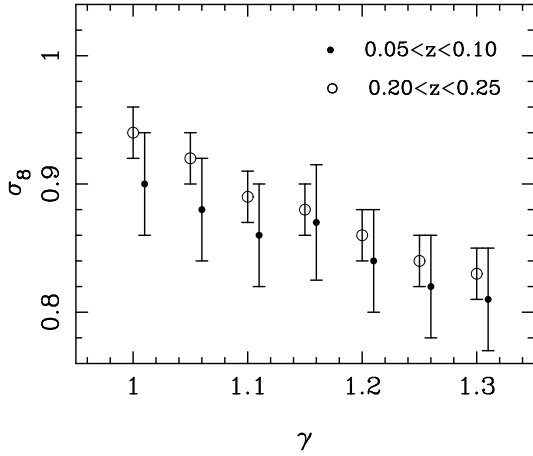


**Figure 7.** The value of  $\sigma_8$  (with  $\Omega_m = 0.3$  fixed) from cluster masses based on the  $M_{\text{vir}}-L_r$  relation varies with a possible systematic bias on mass conversion of  $\gamma = M_{\text{vir}}/M_{\text{vir,true}}$ .

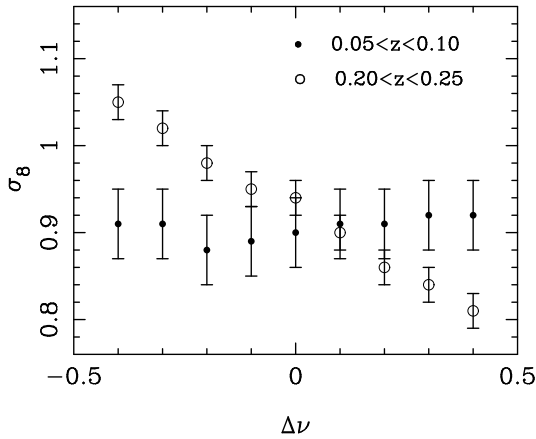


**Figure 8.** The value of  $\sigma_8$  (with  $\Omega_m = 0.3$  fixed) from cluster masses based on the  $M_{\text{vir}}-L_r$  relation varies with a possible systematic bias on the slope of the scaling relation by  $\Delta\nu$ .

$\sigma_8$ . Figure 8 shows the  $\sigma_8$  value varies with  $\Delta\nu$ . We find that the  $\sigma_8$  from the cluster sample of  $0.05 < z < 0.1$  does not change significantly with  $\Delta\nu$ , while the  $\sigma_8$  decreases from 1.05 to 0.81 for the cluster sample of  $0.2 < z < 0.25$  when the slope varies by  $\Delta\nu$  from -0.4 to 0.4.

We can compare our results of  $\sigma_8$  with previous determinations from cluster mass function, as listed in Table 2. Most of previous results are based on X-ray flux-limited cluster samples. Our results are systematically larger than those from the mass function of X-ray clusters.

Roza et al. (2010) used the largest number of clusters from SDSS maxBCG catalog to determine the amplitude of cluster mass function. They did not estimate the mass for each cluster, but gave a statistical mass for clusters within a richness bins by weak lensing. They got  $\sigma_8 = 0.76 \pm 0.03$  assuming  $\Omega_m = 0.30$ . The maxBCG clusters were selected based on the red brightest cluster galaxies (BCGs). However, the maxBCG method may miss about 25% clusters in which the BCGs have emission line and blue colors (Koester et al. 2007). We notice that about 15% rich clusters ( $R \geq 16.7$ ) are missing by the maxBCG method compared to our sample in the redshift range of  $0.2 < z < 0.25$ . However, the

systematic incompleteness only induces an underestimate of 3% for  $\sigma_8$ . Therefore, the discrepancy probably comes from the uncertainty of mass scaling relations.

If we take  $\Omega_m = 0.26$  derived from WMAP7, then our values of  $\sigma_8$  should become larger by a factor of  $(0.26/0.3)^{\sim 0.42} = 1.06$ , roughly equal to adding 0.05 to the our  $\sigma_8$  value in Table 2. Therefore, the  $\sigma_8$  values we derived from galaxy clusters are slightly larger than the those from the WMAP data (Komatsu et al. 2009; Larson et al. 2010). While some reanalysis of the WMAP5 data independently (Li et al. 2009) gives  $\sigma_8 = 0.921 \pm 0.036$  for  $\Omega_m = 0.32 \pm 0.03$  (see Liu & Li 2009). Some studies of cosmic microwave background at small scales also give higher values of  $\sigma_8$  than that from WMAP (Readhead et al. 2004; Dawson et al. 2006; Reichardt et al. 2009; Sievers et al. 2009).

Our result of  $\sigma_8$  are consistent with many recent studies using other methods. For example, the  $\sigma_8$  by weak lensing method has a mean value of  $0.85 \pm 0.03$  (see previous results in Table 5 of Hettterscheidt et al. 2007), which is higher than previous results from X-ray clusters. Tegmark et al. (2004) studied the power spectrum of galaxies from the SDSS to constrain cosmological parameters. They obtained  $\sigma_8 = 0.89 \pm 0.02$  and  $\Omega_m = 0.30 \pm 0.03$ . Lee (2009) studied the normalization of the power spectrum via the ellipticity function of giant galaxy voids from SDSS DR5 and obtained  $\sigma_8 = 0.90 \pm 0.04$ . Jena et al. (2005) used the Ly $\alpha$  data and found  $\sigma_8 = 0.9$  and  $\Omega_m = 0.27$ . Feldman et al. (2003) used the galaxy peculiar velocities to probe the growth rate of the structure and found that  $\sigma_8 = 1.13^{+0.22}_{-0.23}$  and  $\Omega_m = 0.30^{+0.17}_{-0.07}$ .

In this work, we get six values of  $\sigma_8$  by cluster mass function. Basically, the results are consistent. However, the precise value of  $\sigma_8$  is still to be determined since our constraint is not only coupled with  $\Omega_m$ , but also has large uncertainties on the scaling relations.

## ACKNOWLEDGMENTS

We thank the referee Dr. Vincent Eke for helpful comments. The authors are supported by the National Natural Science Foundation (NNSF) of China (10773016, 10821061, and 1083303) and the National Key Basic Research Science Foundation of China (2007CB815403) and the Liaoning Educational Foundation of China (2009A646, XN200902, 054-55440105020). Funding for the SDSS and SDSS-II has been provided by the Alfred P. Sloan Foundation, the Participating Institutions, the National Science Foundation, the U.S. Department of Energy, the National Aeronautics and Space Administration, the Japanese Monbukagakusho, the Max Planck Society, and the Higher Education Funding Council for England. The SDSS Web site is <http://www.sdss.org/>. The SDSS is managed by the Astrophysical Research Consortium for the Participating Institutions. The Participating Institutions are the American Museum of Natural History, Astrophysical Institute Potsdam, University of Basel, Cambridge University, Case Western Reserve University, University of Chicago, Drexel University, Fermilab, the Institute for Advanced Study, the Japan Participation Group, Johns Hopkins University, the Joint Institute for Nuclear Astrophysics, the Kavli Institute for Particle Astrophysics and Cosmology, the Korean Scientist Group, the Chinese Academy of Sciences (LAMOST), Los Alamos National Laboratory, the Max Planck Institute for Astronomy (MPIA), the Max Planck Institute for Astrophysics (MPA), New Mexico State University, Ohio State University, University of Pittsburgh, University of Portsmouth, Princeton University, the United States Naval Observatory, and the University of Washington.

## REFERENCES

- Adelman-McCarthy, J. K., Agüeros, M. A., Allam, S. S., et al. 2008, *ApJS*, 175, 297
- Allen, S. W., Schmidt, R. W., Fabian, A. C., et al. 2003, *MNRAS*, 342, 287
- Arnaud, M., Pointecouteau, E., & Pratt, G. W. 2005, *A&A*, 441, 893
- Bahcall, N. A., Dong, F., Bode, P., et al. 2003, *ApJ*, 585, 182
- Bahcall, N. A. & Fan, X. 1998, *ApJ*, 504, 1
- Bardeau, S., Soucail, G., Kneib, J., et al. 2007, *A&A*, 470, 449
- Benjamin, J., Heymans, C., Semboloni, E., et al. 2007, *MNRAS*, 381, 702
- Blanchard, A., Sadat, R., Bartlett, J. G., et al. 2000, *A&A*, 362, 809
- Borgani, S., Rosati, P., Tozzi, P., et al. 1999, *ApJ*, 517, 40
- Borgani, S., Rosati, P., Tozzi, P., et al. 2001, *ApJ*, 561, 13
- Broadhurst, T., Takada, M., Umetsu, K., et al. 2005, *ApJ*, 619, L143
- Cole, S., Percival, W. J., Peacock, J. A., et al. 2005, *MNRAS*, 362, 505
- Corless, V. L., King, L. J., & Clowe, D. 2009, *MNRAS*, 393, 1235
- Dahle, H. 2006, *ApJ*, 653, 954
- Dahle, H., Pedersen, K., Lilje, P. B., et al. 2003, *ApJ*, 591, 662
- Dawson, K. S., Holzappel, W. L., Carlstrom, J. E., et al. 2006, *ApJ*, 647, 13
- Eke, V. R., Baugh, C. M., Cole, S., et al. 2006, *MNRAS*, 370, 1147
- Eke, V. R., Cole, S., & Frenk, C. S. 1996, *MNRAS*, 282, 263
- Erben, T., van Waerbeke, L., Mellier, Y., et al. 2000, *A&A*, 355, 23
- Feldman, H., Juszkiewicz, R., Ferreira, P., et al. 2003, *ApJ*, 596, L131
- Girardi, M., Borgani, S., Giuricin, G., et al. 1998, *ApJ*, 506, 45
- Girardi, M., Manzato, P., Mezzetti, M., et al. 2002, *ApJ*, 569, 720
- Halkola, A., Seitz, S., & Pannella, M. 2006, *MNRAS*, 372, 1425
- Henry, J. P. 2004, *ApJ*, 609, 603
- Henry, J. P., Evrard, A. E., Hoekstra, H., et al. 2009, *ApJ*, 691, 1307
- Hetterscheidt, M., Simon, P., Schirmer, M., et al. 2007, *A&A*, 468, 859
- Hoekstra, H., Mellier, Y., van Waerbeke, L., et al. 2006, *ApJ*, 647, 116
- Hoekstra, H. 2007, *MNRAS*, 379, 317
- Jena, T., Norman, M. L., Tytler, D., et al. 2005, *MNRAS*, 361, 70
- Jenkins, A., Frenk, C. S., Pearce, F. R., et al. 1998, *ApJ*, 499, 20
- Jenkins, A., Frenk, C. S., White, S. D. M., et al. 2001, *MNRAS*, 321, 372
- Kitayama, T. & Suto, Y. 1996, *ApJ*, 469, 480
- Kitching, T. D., Heavens, A. F., Taylor, A. N., et al. 2007, *MNRAS*, 376, 771
- Koester, B. P., McKay, T. A., Annis, J., et al. 2007, *ApJ*, 660, 239
- Komatsu, E., Dunkley, J., Nolta, M. R., et al. 2009, *ApJS*, 180, 330
- Larson, D., Dunkley, J., Hinshaw, G., et al. 2010, *arXiv:1001.4635*
- Lee, J. 2009, *arXiv:0907.4453*
- Li, T., Liu, H., Song, L., et al. 2009, *MNRAS*, 398, 47
- Lilje, P. B., & Efstathiou, G. 1988, *MNRAS*, 231, 635
- Limousin, M., Richard, J., Jullo, E., et al. 2007, *ApJ*, 668, 643
- Liu, H. & Li, T. 2009, *arXiv:0907.2731*
- Markevitch, M. 1998, *ApJ*, 504, 27
- McDonald, P., Seljak, U., Cen, R., et al. 2005, *ApJ*, 635, 761
- Okabe, N. & Umetsu, K. 2008, *PASJ*, 60, 345
- Oukbir, J. & Arnaud, M. 2001, *MNRAS*, 326, 453
- Pedersen, K. & Dahle, H. 2007, *ApJ*, 667, 26
- Pen, U.-L. 1998, *ApJ*, 498, 60
- Pierpaoli, E., Borgani, S., Scott, D., et al. 2003, *MNRAS*, 342, 163
- Pierpaoli, E., Scott, D., & White, M. 2001, *MNRAS*, 325, 77
- Pointecouteau, E., Arnaud, M., & Pratt, G. W. 2005, *A&A*, 435, 1
- Popesso, P., Biviano, A., Böhringer, H., et al. 2007a, *A&A*, 461, 397
- Popesso, P., Biviano, A., Böhringer, H., et al. 2007b, *A&A*, 464, 451
- Press, W. H. & Schechter, P. 1974, *ApJ*, 187, 425
- Readhead, A. C. S., Mason, B. S., Contaldi, C. R., et al. 2004, *ApJ*, 609, 498
- Reichardt, C. L., Ade, P. A. R., Bock, J. J., et al. 2009, *ApJ*, 694, 1200
- Reiprich, T. H. & Böhringer, H. 2002, *ApJ*, 567, 716
- Rines, K., Diaferio, A., & Natarajan, P. 2007, *ApJ*, 657, 183
- Rozo, E., Wechsler, R. H., Rykoff, E. S., et al. 2010, *ApJ*, 708, 645
- Sayers, J., Golwala, S. R., Rossinot, P., et al. 2009, *ApJ*, 690, 1597
- Schindler, S. 1996, *A&A*, 305, 756
- Schmidt, R. W. & Allen, S. W. 2007, *MNRAS*, 379, 209
- Schuecker, P., Böhringer, H., Collins, C. A., et al. 2003, *A&A*, 398, 867
- Seljak, U. 2002, *MNRAS*, 337, 769
- Sheth, R. K. & Tormen, G. 1999, *MNRAS*, 308, 119
- Shimizu, M., Kitayama, T., Sasaki, S., et al. 2003, *ApJ*, 590, 197
- Sievers, J. L., Mason, B. S., Weintraub, L., et al. 2009, *arXiv:0901.4540*
- Spergel, D. N., Bean, R., Doré, O., et al. 2007, *ApJS*, 170, 377
- Spergel, D. N., Verde, L., Peiris, H. V., et al. 2003, *ApJS*, 148, 175
- Sun, M., Voit, G. M., Donahue, M., et al. 2009, *ApJ*, 693, 1142
- Tegmark, M., Blanton, M. R., Strauss, M. A., et al. 2004, *ApJ*, 606, 702
- Umetsu, K., & Broadhurst, T. 2008, *ApJ*, 684, 177
- Veneziani, M., Amblard, A., Cooray, A., et al. 2009, *ApJ*, 702, L61
- Viana, P. T. P., Kay, S. T., Liddle, A. R., et al. 2003, *MNRAS*, 346, 319
- Viana, P. T. P. & Liddle, A. R. 1996, *MNRAS*, 281, 323
- . 1999, *MNRAS*, 303, 535
- Viana, P. T. P., Nichol, R. C., & Liddle, A. R. 2002, *ApJ*, 569, L75
- Vikhlinin, A., Kravtsov, A., Forman, W., et al. 2006, *ApJ*, 640, 691
- Vikhlinin, A., Kravtsov, A. V., Burenin, R. A., et al. 2009, *ApJ*, 692, 1060
- von der Linden, A., Best, P. N., Kauffmann, G., et al. 2007, *MNRAS*, 379, 867
- Warren, M. S., Abazajian, K., Holz, D. E., et al. 2006, *ApJ*, 646, 881
- Wen, Z. L., Han, J. L., & Liu, F. S. 2009, *ApJS*, 183, 197
- White, S. D. M., Efstathiou, G., & Frenk, C. S. 1993, *MNRAS*, 262, 1023
- Wu, J.-H. P. 2001, *MNRAS*, 327, 629
- Xu, H., Jin, G., & Wu, X.-P. 2001, *ApJ*, 553, 78
- Yee, H. K. C. & Ellingson, E. 2003, *ApJ*, 585, 215
- Zhang, Y., Finoguenov, A., Böhringer, H., et al. 2007, *A&A*, 467, 437
- Zwicky, F. 1933, *Helvetica Physica Acta*, 6, 110